Electronic Supplementary Material (ESI) for RSC Advances.

Supporting information

Investigation on cation distribution and luminescence in spinel phase γ-$Ga_{3-\delta}O_4$:Sm nanostructures using X-ray absorption spectroscopy

Aditya Sharma[a*], Mayora Varshney[a], Hyun-Joon Shin[b], Keun Hwa Chae[a], Sung Ok Won[a*]

[a] Advanced Analysis Centre, Korea Institute of Science and Technology, Seoul -02792, South Korea

[b] Pohang Accelerator Laboratory (POSTECH), Pohang – 37673, South Korea

1. Raman Study

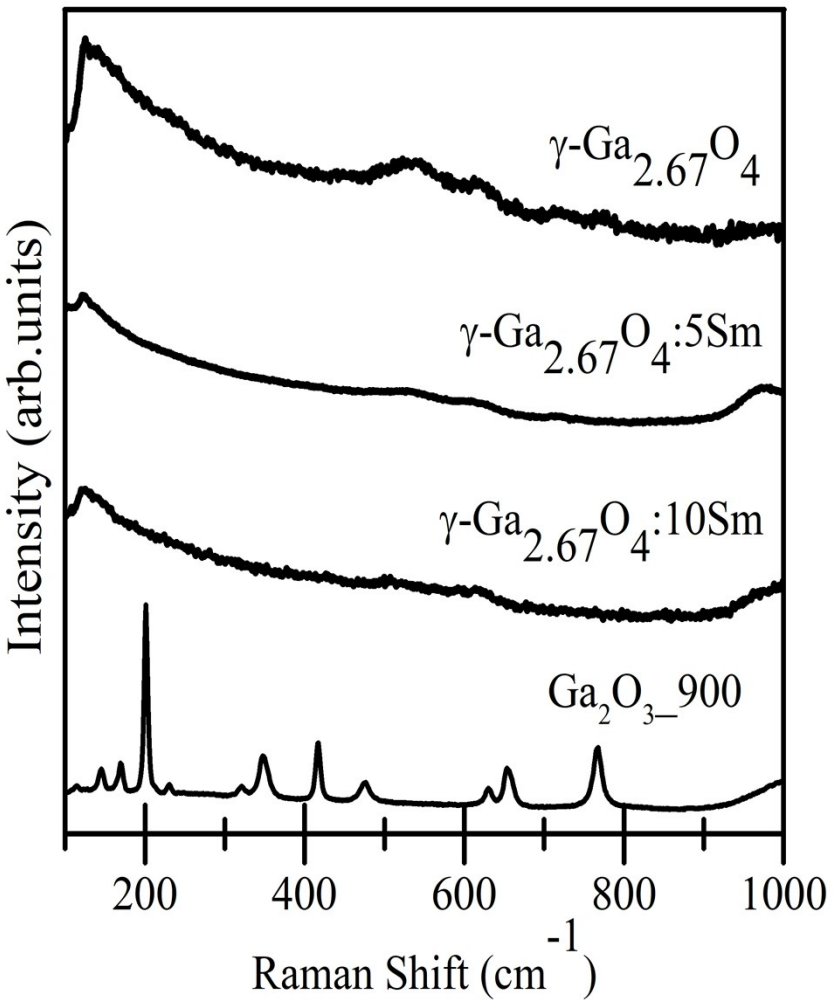

Figure. S1. Raman spectra of pure γ-$Ga_{2.67}O_4$, γ-$Ga_{2.67}O_4$:5Sm, γ-$Ga_{2.67}O_4$:10Sm, Ga_2O_3 _900 samples. Spectra are vertically moved for the clarity of data.

It can be seen from the Figure S1 that pure γ-$Ga_{2.67}O_4$ sample has some weak and broad bands around 530 cm^{-1} and 615 cm^{-1}. These broad bands are attributed to the bending and stretching of the Ga-O bonds [R1-R2]. The appearance of weak band could be due to the narrow size of the as prepared γ-$Ga_{2.67}O_4$ nanocomposites. Furthermore, the intensity of Ga-O Raman bands is progressively weakened with increasing the Sm doping concentrations. This reduction in the Ga-O Raman band intensity may be attributed to the distortion in the Ga-O local lattice in the narrower sized γ-$Ga_{2.67}O_4$:Sm nanocomposites. XRD pattern of γ-$Ga_{2.67}O_4$:Sm nanocomposites have also exhibited the structural disorders in the γ-$Ga_{2.67}O_4$ lattice and tally our Raman spectra. In the lower panel of Fig. S1, we have presented the Raman modes of β-Ga_2O_3 phase (i.e., Ga_2O_3_900 sample) for the comparing the Raman spectra of γ-$Ga_{2.67}O_4$:Sm samples. One can see that none of the Raman modes from the γ-$Ga_{2.67}O_4$:Sm nano composites are matching with the Raman modes of Ga_2O_3_900 and, thus, nullifying the formation of lower symmetric polymorphous phases under the Sm doping in γ-$Ga_{2.67}O_4$. The Sm insertion has only affected the local structural properties but the cubic phase of γ-$Ga_{2.67}O_4$ was persistent in the higher Sm concentration doped sample. In contrary to the cubic γ-$Ga_{2.67}O_4$, the monoclinic β-Ga_2O_3 is exhibiting several Raman active modes. The monoclinic unit cell of β-Ga_2O_3 offers 15 Raman and 12 infrared IR active modes because of diverse octahedral and tetrahedral position of Ga atoms [R1-R2]. In contrary to the γ-$Ga_{2.67}O_4$ the β-Ga_2O_3 is extensively studied by the Raman spectroscopy. Based on the theoretical and experimental findings, the Raman modes of β-Ga_2O_3 has been classified into three groups; (i) high-frequency stretching and bending of Ga-O4 tetrahedra (770–500 cm^{-1}), (ii) mid-frequency deformation of Ga2-O6 octahedra (480–310 cm^{-1}) and (iii) low frequency libration and translation (below 200 cm^{-1}) of tetrahedra-octahedra chains [R1-R2]. In the present study, the Raman active modes are appeared at; 113.2 cm^{-1}, 117.4 cm^{-1}, 144.5 cm^{-1}, 169.7 cm^{-1}, 200.4 cm^{-1}, 230.8 cm^{-1}, 320.5 cm^{-1}, 348.1 cm^{-1}, 415.7 cm^{-1}, 475.7 cm^{-1}, 630.9 cm^{-1}, 654.1 cm^{-1} and 767.6 cm^{-1}. The position of Raman active modes of Ga_2O_3_900 sample is in accordance with the previous reports on the β-Ga_2O_3 phase [R1-R2] and, hence, further convince the formation of pure β-Ga_2O_3 crystals upon annealing the γ-$Ga_{2.67}O_4$ nanoparticles.

2. TEM study

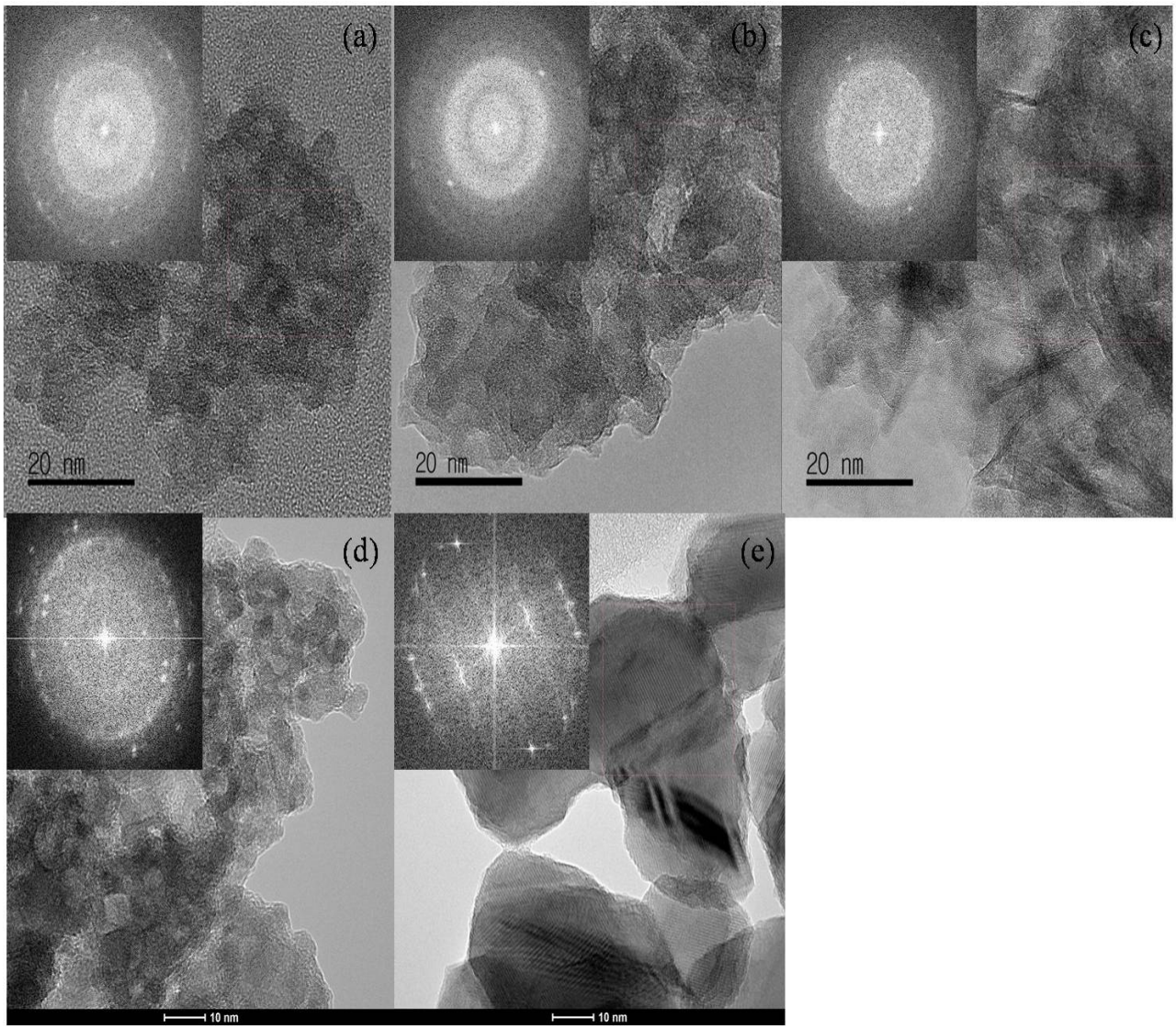

Figure S2. TEM images of (a) pure γ-$Ga_{2.67}O_4$, (b) γ-$Ga_{2.67}O_4$:5Sm, (c) γ-$Ga_{2.67}O_4$:10Sm (d) Ga_2O_3_600 and (e) Ga_2O_3_900 samples, respectively.

It is noticeable from the Fig. S2 that pure and Sm doped samples exhibit aggregated nanoparticle morphology without any special geometry (i.e., nanorod, nanotube, nanowire etc.). The aggregation in the samples is expected due to the presence of sufficient amount of hydroxyl ions in the chemically synthesized samples. The pure γ-$Ga_{2.67}O_4$ sample has exhibited reasonable intense FFT rings and conveying a moderate crystallinity in the sample. The low intensity of FFT(Fig. S2 (b) and (c)) rings suggests the lower crystallinity and/or small size in the Sm doped sample and tallies our XRD and Raman results. A significant dwindling in the size/shape of particles is also visible from the TEM images of Sm doped samples and convincing our XRD studies. The increase in the particle size is seen

in the Ga_2O_3_600 and (e) Ga_2O_3_900 samples. Besides the particle size enhancement in the annealed samples, the FFT rings are also intensified with increasing the annealing temperature and signifying the superior crystallinity in the higher temperature annealed samples.

3. Ga L-edge and Sm M-edge study

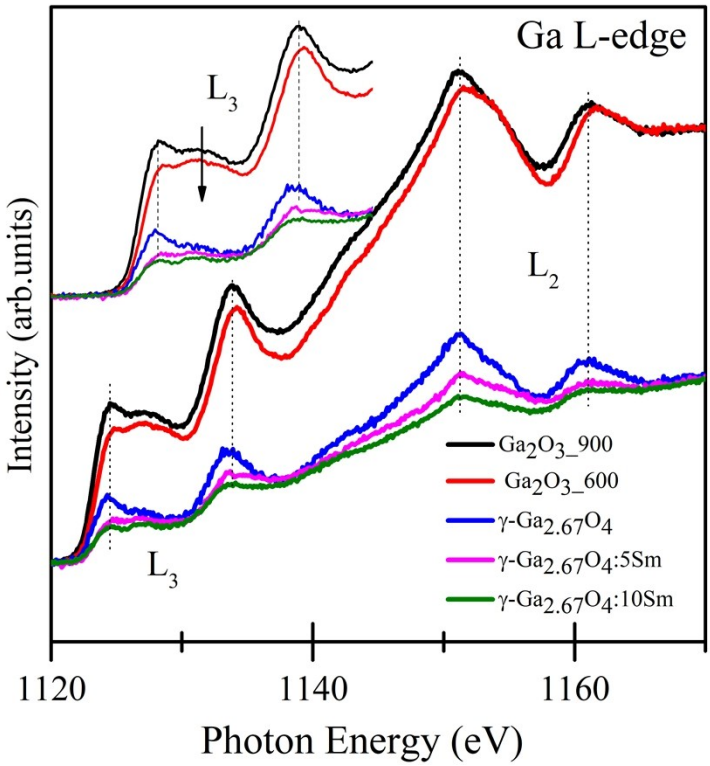

Figure S4. Ga L-edge XANES of pure γ-$Ga_{2.67}O_4$, γ-$Ga_{2.67}O_4$:5Sm, γ-$Ga_{2.67}O_4$:10Sm, Ga_2O_3_600 and Ga_2O_3_900 samples.

Fig. S4 shows the Ga $L_{3,2}$-edge XANES spectra from the samples. The first two spectral features (between the 1120 eV - 1140 eV) are known as L_3-edge and the higher energy features (between the 1150 eV to 1170 eV) are known as L_2-edge [R3-R4]. The spectral features of all of the samples are nearly similar to each other and resembled to the previously reported Ga L-edge spectra of gallium oxide with +3 oxidation state [R3-R4]. The minor differences can be seen in the L_3-edge spectra of γ phase samples (i.e., γ-$Ga_{2.67}O_4$, γ-$Ga_{2.67}O_4$:5Sm, γ-$Ga_{2.67}O_4$:10Sm) and β phase samples (i.e., Ga_2O_3_600 and Ga_2O_3_900). For the clarity, we have shown a magnified view of L_3-edge features in the inset of Fig. S4. It is noticeable from the inset of Fig. S4 that the β phase samples show a post-edge feature (marked by arrow), however, such features are also certainly present in the γ-$Ga_{2.67}O_4$ samples, especially, in the Sm doped samples. Based on the previous reports on gallium oxide polymorphous

samples [R3], the α-Ga_2O_3 (which has dominating octahedral occupancy of Ga atoms) has exhibited only sharp L_3-edge peak. In contrary to the L-edge XANES of α-Ga_2O_3, the spectral features of β-Ga_2O_3 have reflected the distinct post edge features [R4]. The origin of L_3 post-edge features was ascribed to the low-coordinated gallium with the oxygen [R4]. In the present study, Sm doped γ-$Ga_{2.67}O_4$ sample has noticeable intensity of such post edge features, however not well resolved under the resolution limit of used beam line. The existence of post-edge features in the Sm doped samples are convincing the low coordinated Ga species and in accordance with the Ga K-edge XANES/EXAFS results. However, we may not provide quantitative analysis of Ga L-edge XANES because of the less resolved spectral feature in the present data set.

Figure S5 shows the Sm M5,4-edge XANES spectra of γ-$Ga_{2.67}O_4$:5Sm and γ-$Ga_{2.67}O_4$:10Sm samples. We have also simulated the Sm M5,4-edge XANES spectra by using the atomic-multiplet calculations for the Sm^{2+} and Sm^{3+} ions and the spectra are shown in the inset of Fig. S5. The CTM4XAS program package [R5] was used to obtain such spectra. In order to simulate the resolution of discrete lines of atomic multiplets, the spectral lines have been broadened with a Lorentzian width of 0.08 eV and a Gaussian width of 0.2 eV. The Slater integral were kept to their default values (i.e., 80% of their Hartree-Fock values). The Sm $M_{5,4}$-edge experimental spectra of γ-$Ga_{2.67}O_4$:5Sm and γ-$Ga_{2.67}O_4$:10Sm samples are fairly similar to each other, escape of higher intensity for the γ-$Ga_{2.67}O_4$:10Sm sample. Intensification of the spectral features is due to the higher concentration of Sm in this sample. The simulated Sm $M_{5,4}$-edge spectral features show distinct differences in the spectral features and edge-energy position. The spectra of Sm^{2+} samples show low energy shifting of M_5 and M_4-edges with respect to the Sm^{3+} spectra. Moreover, the presence of intense M_5-edge peak absence of pre- M4-edge feature can be seen in the Sm^{2+} simulated spectrum, while compared with the Sm^{3+} simulated spectrum (marked by arrows). The pre- M4-edge feature is present in experimental XANES and the post-edge of the M5 peak is also not much intense. The spectral features of experimental M5,4-edge XANES may convey that the Sm3+ ions are the favorable species in the γ-$Ga_{2.67}O_4$:5Sm and γ-$Ga_{2.67}O_4$:10Sm and Sm2+ ions may not likely present in the samples, as recommended by Sm L-edge XANES.

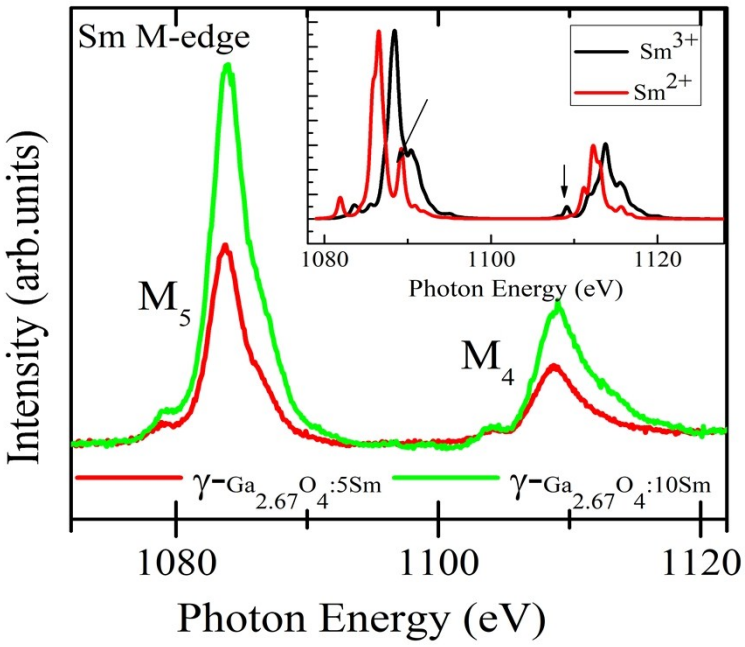

Figure S5. Sm M5,4-edge XANES of γ-$Ga_{2.67}O_4$:5Sm and γ-$Ga_{2.67}O_4$:10Sm samples. The inset shows the multiplet-calculation simulated Sm $M_{5,4}$-edge spectra for Sm^{3+} and Sm^{2+}.

4. Details of Ga K-edge analysis

The Ga K-edge XANES spectra were analyzed by de-convolution of white line region (i.e., 10355 eV to 10385 eV). During the simulations, we assumed that the spectrum is consisting two components. Each component assigned to have one Gaussian curve for white line and an arctangent curve for continuum absorption. The energy of inflection point of arctangent curve is kept the same as that of the corresponding Gaussian curve. The ratio of the height of the each arctangent curve is taken to equal (or within ± 10% errors) to the ratio of the peak area of each Gaussian curve to achieve better fittings. In the following Table S1, parameters of deconvoluted peaks are presented along with the fractional percentage of Ga(t) and Ga(o). The fractional percentages of Ga(t) and Ga(o) were calculated by using the area of Gaussian 1(Ga(t)) and area of Gaussian 2 (Ga (o)).

(i) To evaluate the fraction of Ga(t)%, we have applied the area ratios in following manner;

$$Ga(t)\% = \frac{\text{Area of Gaussian 1}}{(\text{Area of Gaussian 1} + \text{Area of Gaussian 2})} \times 100$$

(ii) Similarly, to evaluate the fraction of Ga(o)%, we have applied the area ratio;

$$Ga(o)\% = \frac{\text{Area of Gaussia 2}}{(\text{Area of Gaussian 1} + \text{Area of Gaussian 2})} \times 100$$

Table S1. Parameters of deconvoluted peaks in Ga K-edge XANES.

Sample Name	Gaussian 1 for Ga(t)/(eV)			Gaussian 2 for Ga(o)/(eV)			Area Ga(t) + Ga(o)	Fraction of Ga(t)%	Fraction of Ga(o)%
	Position	FWHM	Area	Position	FWHM	Area			
Ga_2O_3_900	10368.5	6.3(5)	4.9(9)	10372.5	8.4(7)	5.3(2)	10.3(1)	48.3(9)	51.6(0)
γ-$Ga_{2.67}O_4$	10368.6	5.1(8)	13.4(1)	10372.6	5.4(1)	9.4(1)	22.8(2)	58.7(6)	41.2(3)
γ-$Ga_{2.67}O_4$:5Sm	10368.9	6.1(2)	12.6(2)	10372.8	6.5(9)	8.3(1)	20.9(3)	60.2(9)	39.7(0)
γ-$Ga_{2.67}O_4$:10Sm	10368.7	7.0(6)	14.0(2)	10372.8	8.2(4)	8.4(1)	22.4(3)	62.5(0)	37.4(9)

The values in parenthesis represent errors therein.

From the Table S1, it is clear that the peak position of Gaussian 1 is nearly the same for all of the samples (i.e., 10368.6 ±0.3). Similarly, the energy position of Gaussian 2 is also nearly the same for all of the samples (i.e., 10372.6±0.2 eV). The calculated fractional Ga(t) and Ga(o) percentages are also reasonable with respect to the reported values (references 48-49 in the main text).

5. Details of EXAFS data simulations

First, the ATHENA was used to subtract the smooth pre-edge function from μ(E) to get rid of the background. The threshold energy E_0 was identified by clicking the maximum of derivative of the absorption coefficient (δμ/δE). The edge-jump was determined at E_0 and normalized so that the pre-edge subtracted and normalized μ(E) was going nearly to 0, below to E_0, to 1 well above the E_0. We also removed the post-edge background function. For this, we used enough long normalization energy range to get the line to go pretty much through the oscillations right the middle straight line. It was also essentially parallel to the pre-edge normalization line. Then, the oscillations were k^3-weighted. All of the data set were also aligned and calibrated. The R_{bkg} was kept 1 for of the data set.

The k^3 weighted EXAFS functions were Fourier transformed (FT) from k-space to r-space to generate the χ(R) versus R (or FT-EXAFS), using ATHENA-ARTEMIS. To simulate the FT-EXAFS data of the pure γ-$Ga_{2.67}O_4$ and γ-$Ga_{2.67}O_4$:Sm samples, a theoretical structure of γ-$Ga_{2.67}O_4$ (space group Fd-3m; a = b = c= 8.22 Å, α=β=γ=90°) was generated using the ATOM/FEFF codes. Ga and O atomic position were taken as to the JCPDS#15-2085, as conveyed by our XRD analysis, which recommends the distribution of Ga^{3+} ions over the two tetrahedral sites (i.e., (8a) and (48f)) and one octahedral (16c) site. Similarly, the EXAFS data of Ga_2O_3_900 sample was simulated with the monoclinic structure (space group C2/m, a = 12.23Å, b=3.04Å, c= 5.8Å, α=90°, β= 103.7°, γ=90°). The atomic positions for this sample were taken as to the JCPDS#04-002-2603 for the β-Ga_2O_3 phase. The data range taken for the FT was 2–12 $Å^{-1}$ in the k-space, and the fittings were performed, in the r-space, within the interval of 1–5 Å. A window function, between 1–5 Å, has also been applied to simulate the EXAFS data. Single scattering paths (Ga-O and Ga-Ga) were taken for the data simulations, however few multiple scattering paths (Ga-O-Ga) were also considered to achieve better fittings (especially in Ga_2O_3-900 °C). During the fittings, the SO^2 (amplitude reduction factor) was kept 0.9 for all samples and E_0 were kept constant (i.e., '*define*') for all of the paths of a certain sample. The R factors of respective fitting were in between 0.01 - 0.03. In such calculations, number of variables was definitely less than the number of independent points. The corrected χ(R) vs. R and phase χ(k) vs. k spectra are presented in the Fig. S6.

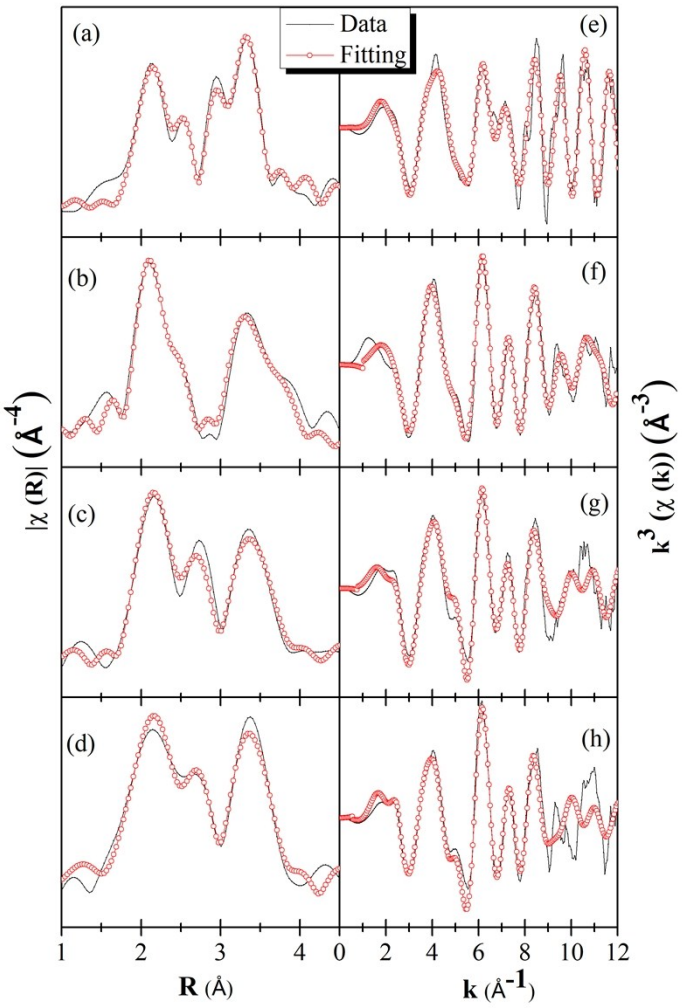

Figure S6. Phase corrected, χ(R) vs. R spectra of; (a) Ga_2O_3_900, (b) γ-$Ga_{2.67}O_4$, (c) γ-$Ga_{2.67}O_4$:5Sm and (d) γ-$Ga_{2.67}O_4$:10Sm, respectively. χ(k) vs. k spectra of (e) Ga_2O_3_900, (f) γ-$Ga_{2.67}O_4$, (g) γ-$Ga_{2.67}O_4$:5Sm and (h) γ-$Ga_{2.67}O_4$:10Sm, respectively.

References for the supporting information

R1. Y. Hou, L. Wu, X. Wang, Z. Ding, Z. Li and X. Fu, J. Catal., 2007, **250**, 12.

R2. R. Rao, A. M. Rao, B. Xu, J. Dong and M. K. Sunkara, J. Appl. Phys., 2005, **98**, 094312.

R3. X. T. Zhou, F. Heigl, J. Y. P. Ko, M. W. Murphy, J. G. Zhou, T. Regier, R. I. R. Blyth, and T. K. Sham, Phys. Rev. B, 2007, **75**, 125303.

R4. K. Shimizu, M. Takamatsu, K. Nishi, H. Yoshida, A. Satsuma, and T. Hattori, Chem. Commun., (Cambridge), 1996, **1827**, 1996.

R5. E. Stavitski and F. M. F. de Groot, Micron, 2010**, 41**, 687

R6. M. Newville, Rev. Miner. Geochem., 2014, 78, 33-74.